Infrared lattice spectra of $Tm_3Al_5O_{12}$ and $Yb_3Al_5O_{12}$ single crystals

2002 J. Phys.: Condens. Matter 14 915

(http://iopscience.iop.org/0953-8984/14/4/323)

INSTITUTE OF PHYSICS PUBLISHING JOURNAL OF PHYSICS: CONDENSED MATTER

J. Phys.: Condens. Matter **14** (2002) 915–923 PII: S0953-8984(02)30975-5

Infrared lattice spectra of $Tm_3Al_5O_{12}$ and $Yb_3Al_5O_{12}$ single crystals

K Papagelis[1], G Kanellis[1], T Zorba[1], S Ves[1,3] and G A Kourouklis[2]

[1] Physics Department, Aristotle University of Thessaloniki, GR-540 06 Thessaloniki, Greece
[2] Physics Division, School of Technology, Aristotle University of Thessaloniki, GR-540 06 Thessaloniki, Greece

E-mail: ves@auth.gr

Received 20 November 2001
Published 18 January 2002
Online at stacks.iop.org/JPhysCM/14/915

Abstract

The reflectance spectra of the $Tm_3Al_5O_{12}$ and $Yb_3Al_5O_{12}$ single crystals have been studied at room temperature. Fifteen infrared-active modes, out of the 17 theoretically predicted, have been experimentally observed. The infrared data have been analysed by means of the Kramers–Kronig transformation to yield the complex dielectric function, the complex refractive index, the absorption coefficient, as well as the frequencies of the longitudinal (ω_{LO}) and transverse (ω_{TO}) long-wavelength T_{1u} modes. Furthermore, the experimental data are compared and discussed in the light of theoretical lattice dynamical calculations based on the rigid-ion model.

1. Introduction

$Tm_3Al_5O_{12}$ and $Yb_3Al_5O_{12}$ belong to the crystal family of the rare-earth aluminium garnets ($RE_3Al_5O_{12}$, RE = rare earth or yttrium). They are synthetic insulators and technologically play an important role as host crystals for near-infrared solid-state lasers [1]—for example, Nd:$Y_3Al_5O_{12}$ is the most popular solid-state laser at present. Despite the high symmetry (cubic), the crystal structure of the rare-earth aluminium garnets is quite complicated (80 atoms per primitive cell), giving rise to a very rich infrared (IR) and Raman spectrum (17 IR-active and 25 Raman-active modes are expected). IR powder absorption spectra for various $RE_3Al_5O_{12}$ compounds and single-crystal IR reflectance measurements for $Y_3Al_5O_{12}$ at room temperature were first reported a long time ago [2, 3]. Later, Hofmeister and Campbell [4] reported the existence of two additional weak peaks which completed the set of expected IR modes for $Y_3Al_5O_{12}$. The vibrational spectra of the garnet crystals as well as their interpretation present, even today, aspects which need clarification. In particular, there is no agreement on the assignment of the bands in terms of the various molecular unit modes. Recently, we

[3] Author to whom any correspondence should be addressed.

have performed lattice dynamical calculations [5] based on the rigid-ion model (RIM) for $Tm_3Al_5O_{12}$ and $Yb_3Al_5O_{12}$, which has allowed us to determine the Raman mode eigenvectors, and the nature and strength of the bonds in these compounds. Moreover, we have managed to clarify the frequency positions for the Raman modes, which do not appear in the experimental spectra.

So far, no single-crystal IR reflectance measurements have been reported for $Tm_3Al_5O_{12}$ and $Yb_3Al_5O_{12}$. Single-crystal IR experimental data would provide more reliable experimental data as far as the values of the frequencies is concerned, since large frequency shifts might occur between the single-crystal reflection and powder absorption frequencies.

In this study we present for the first time single-crystal reflectance measurements on $Tm_3Al_5O_{12}$ and $Yb_3Al_5O_{12}$. From their Kramers–Kronig analysis we determined clearly 15 IR modes, while the missing two are calculated using the RIM model. The effective charges of the ions along with the force constants of the bonds between the cations and oxygens in the basic polyhedra of the garnet structure have been calculated. Also the ω_{LO}–ω_{TO} splitting has been estimated.

2. Experimental details

The single-crystal $Tm_3Al_5O_{12}$ and $Yb_3Al_5O_{12}$ samples were grown by the Czochralski technique and were made available to us by VanUitert and Jayaraman of AT&T Bell Laboratories. FTIR measurements were carried out at room temperature with a Bruker vacuum spectrometer, IFS113v. All the spectra from unoriented, polished single-crystal samples, were collected in reflectance mode at room temperature in the spectral range between 100 and 5000 cm^{-1} (MIR and FIR regions). The resolution was 2 cm^{-1} and for each spectrum 64 consecutive scans were recorded.

3. Results and discussion

The garnet crystal structure belongs to the space group $Ia3d$ (O_h^{10}) [6] and crystallizes in the body-centred cubic Bravais lattice. The 80 atoms contained in the primitive cell are distributed in the following way: (i) 8 Al ions are located at octahedral sites; (ii) 12 Al ions occupy tetrahedral sites; (iii) 12 RE ions occupy dodecahedral sites; and (iv) 48 oxygens are located at general positions. Therefore, the garnet crystal structure consists of a three-dimensional network of polyhedra (tetrahedra, octahedra, and dodecahedra) having an appropriate cation at their centres and surrounded by the appropriate number of oxygen ions [5]. Each oxygen belongs to two dodecahedra, one tetrahedron, and one octahedron. The tetrahedral Al–O distance is ∼1.77 Å, the octahedral Al–O one is ∼1.94 Å, while the dodecahedral RE–O one is ∼2.30 Å.

Group theory analysis, for the garnet structure, predicts 17 triply degenerate T_{1u} modes which are IR active. The degeneracy of the IR-active modes is partially removed under the influence of long-range electrostatic forces, with each mode giving rise to a single longitudinal vibration (LO) and a doubly degenerate transverse vibration (TO). Figure 1 shows the expanded reflection spectra for $Tm_3Al_5O_{12}$ and $Yb_3Al_5O_{12}$ in the range 100–950 cm^{-1}. The insets depict the spectra over the whole energy region investigated. As can be seen, above 2000 cm^{-1} a nearly flat reflectance is observed. The shoulder at ∼105 cm^{-1} shown in the reflectance spectrum of $Yb_3Al_5O_{12}$ is an artifact of the apparatus and has been discarded. The experimental spectra resemble those of other garnet single crystals, e.g. of $Y_3Al_5O_{12}$ [3, 4]. For both materials investigated, the experimental spectra exhibit 15 well-resolved reflectance peaks. It

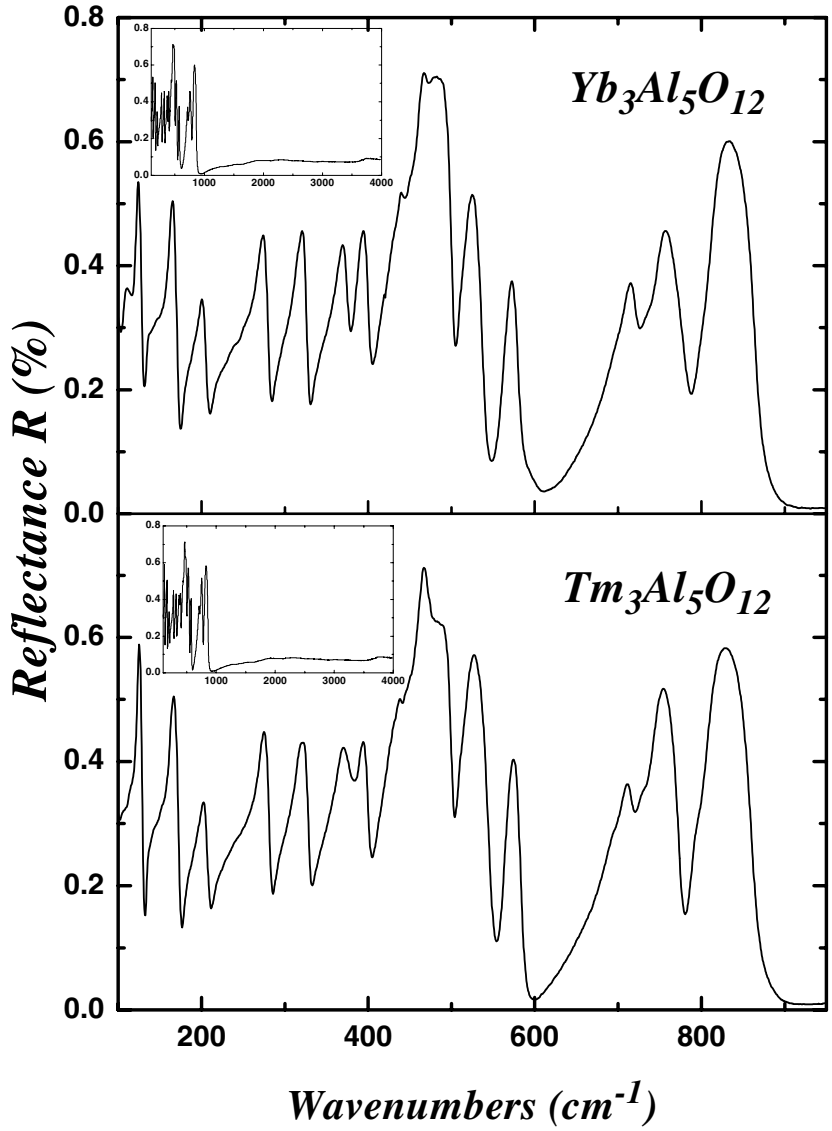

Figure 1. Single-crystal reflectance spectra for $Tm_3Al_5O_{12}$ and $Yb_3Al_5O_{12}$. The insets show the spectra over the whole region investigated in this study.

is worth noting that the high-frequency region (600–800 cm^{-1}) is well separated by a reflection minimum from the rest of the spectral region and contains three bands. This fact is in agreement with our theoretical prediction [5] that the one-phonon density of states, in the rare-earth aluminium garnets, shows a frequency gap in the region 640–690 cm^{-1}. Finally, each material exhibits a strong reflectance maximum in the 400–500 cm^{-1} region.

The real, $\varepsilon_1(\omega)$, and imaginary, $\varepsilon_2(\omega)$, parts of the dielectric function, the real, $n_1(\omega)$, and the imaginary $\kappa_1(\omega)$, parts of the refractive index, as well as the absorption coefficient as obtained by Kramers–Kronig transformation are presented in figures 2–4, respectively. The experimental frequency values of the transverse (ω_{TO}) and longitudinal (ω_{LO}) modes derived from the peak positions of $\varepsilon_2(\omega)$ and $\mathrm{Im}\,(1/\tilde{\varepsilon}(\omega))$, respectively, are listed in table 1. For

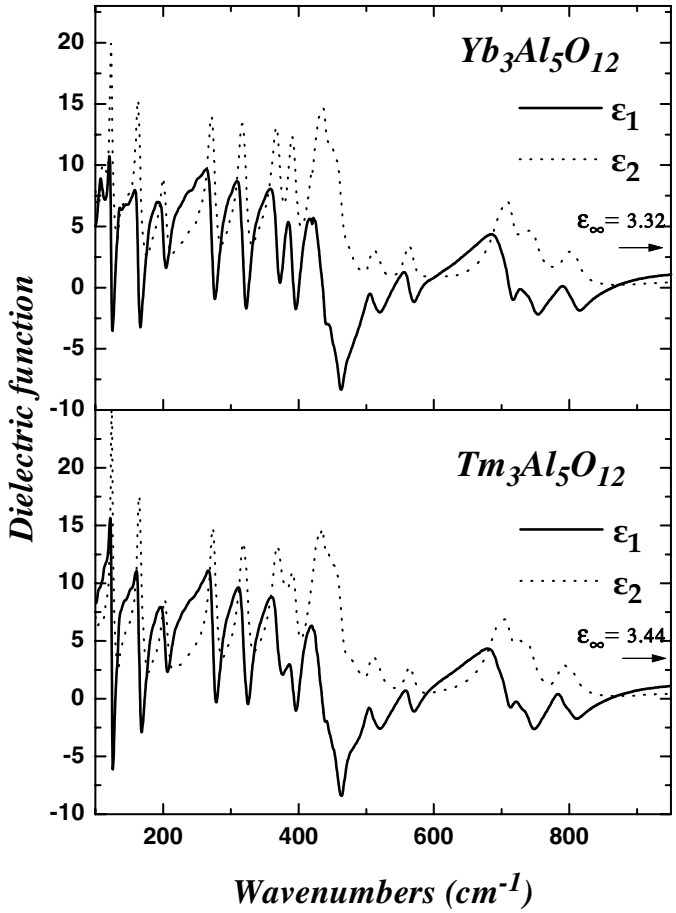

Figure 2. The real (ε_1) and imaginary (ε_2) parts of the dielectric constant derived from Kramers–Kronig analysis for the $Tm_3Al_5O_{12}$ and $Yb_3Al_5O_{12}$ single crystals.

completeness we have included the phonon frequencies obtained by absorption measurements on powder samples [2], where a clear overestimation of the ω_{TO}-frequencies is apparent.

As has already been mentioned above, we observe 15 IR-active modes. The two missing modes are probably very weak and/or lying close to strong peaks, and as a result are not resolved. The latter is more likely for the peak at $\sim$376 cm^{-1}, as it lies in the region between the strong peaks at 368 and 392 cm^{-1}. This assumption is further supported by the $Y_3Al_5O_{12}$ case, where the existence of two additional narrow and weak bands at 176 and 386 cm^{-1} has been reported [4], thus completing the set of the IR modes for the $Y_3Al_5O_{12}$ compound. Therefore, in order to obtain a better understanding of the vibrational mode characteristics as well as to elucidate the problem of the frequency position of the two missing modes, we have carried out lattice dynamical calculations for the $Tm_3Al_5O_{12}$ and $Yb_3Al_5O_{12}$ crystals using the RIM. The details of our nine-parameter RIM have been described in [5]. In this work the short-range forces up to the fourth neighbour are described by the Born–Mayer potential while the long-range electrostatic forces are calculated by the Ewald method [7]. The calculated eigenfrequency values are summarized in table 1. The theoretical ω_{LO}-frequencies have been obtained by applying the macroscopic field along the $\langle 100 \rangle$ direction of the Brillouin zone.

Table 1. Experimental and calculated frequencies of the IR-active modes of $Tm_3Al_5O_{12}$ and $Yb_3Al_5O_{12}$ single crystals obtained by the use of the RIM. The ω_{LO}-values have been calculated taking the macroscopic field to be in the ⟨100⟩ direction of the Brillouin zone.

$Tm_3Al_5O_{12}$					$Yb_3Al_5O_{12}$				
Experiment (cm^{-1})			Theory (cm^{-1})		Experiment (cm^{-1})			Theory (cm^{-1})	
ω_{TO}	ω_{LO}	ω^a	ω_{TO}	ω_{LO}	ω_{TO}	ω_{LO}	ω^a	ω_{TO}	ω_{LO}
—	—	92	96.3	96.3	—	—	92	96.1	96.2
123.3	130.3	126	121.4	123.7	122.9	129.8	125	121.5	123.6
164.2	173.7	167	156.1	156.5	162.5	172.1	165	158.8	159.6
201.8	208.2	201	196.1	196.3	200.0	206.8	202	195.1	195.3
273.2	282.6	279	266.8	285.7	270.9	281.4	278	269.0	289.1
318.9	329.8	323	307.5	313.2	316.7	328.1	322	307.8	313.6
368.4	380.6	371	365.4	368.3	366.5	376.5	372	365.9	368.0
—	—	—	375.5	380.5	—	—	—	377.5	382.1
392.1	401.8	397	388.3	404.7	390.6	402.3	397	386.9	402.3
432.2	445.1	—	414.8	414.9	434.1	449.2	—	423.2	424.2
449.4	481.6	440	458.2	461.3	448.9	475.9	439	462.9	463.0
475.0	501.9	463	476.5	495.9	469.7	502.5	468	468.8	497.0
510.3	546.8	518	509.5	561.4	511.4	539.5	516	513.9	560.4
564.2	584.5	570	574.4	602.2	563.0	582.7	569	572.5	600.4
704.8	717.8	700	701.2	718.2	708.0	723.7	709	707.8	723.6
725.5	774.6	737	720.8	758.0	737.8	781.3	742	726.7	764.8
791.0	860.1	800	784.8	906.2	800.7	864.0	805	790.6	907.5

[a] Powder data from [2].

A similar calculation for the field along the ⟨110⟩ shows negligible difference. In the fitting procedure we have used all the experimental Raman and TO IR frequencies[4]. The agreement between the experimental and theoretical values of the ω_{TO}- as well as of the ω_{LO}-frequencies is very satisfactory. The only discrepancy is the overestimation of the LO–TO splitting for the highest-frequency mode. The reason for this discrepancy is not clear, but this is most probably due to the fact that only the experimental values of ω_{TO} have been used in the fitting procedure (see footnote 4). The calculated values of the effective charges as well as the bond-stretching (L) and bond-bending (T) force constants for the various bond configurations are listed in table 2. It is evident that the short-range bond-stretching force constants L_{tetr} are almost double the corresponding constants L_{oct} and L_{dod}. The same is true for bond-bending force constants but their absolute values are an order of magnitude smaller than those of the stretching ones. Finally, by considering the force constants L and T along with the estimated effective charges in the octahedral and dodecahedral configurations, we infer that the tetrahedral Al–O bonds exhibit mostly a covalent character, while the dodecahedral RE–O bonds have rather an ionic character. It is worth mentioning that the values of the force constants and the effective charges obtained in this study are very close to the ones reported earlier [5]. The standard deviation between the calculated and experimental values of the frequencies is improved by about 10% with respect to our previous results [5] (in the present calculation, $\sigma \sim 9.3$ and 10.8 cm^{-1} for $Tm_3Al_5O_{12}$ and $Yb_3Al_5O_{12}$, respectively).

[4] We have used in the fitting procedure only the experimental frequencies ω_{TO} because of uncertainties in the assignment of the experimental ω_{LO}-values to the corresponding branches. Due to the lowering of the wavevector symmetry for the various Brillouin zone directions caused by applying the macroscopic field, one gets contributions from many zone-centre irreducible representations. Therefore, very accurate experimental dispersion data are necessary in order to resolve this problem.

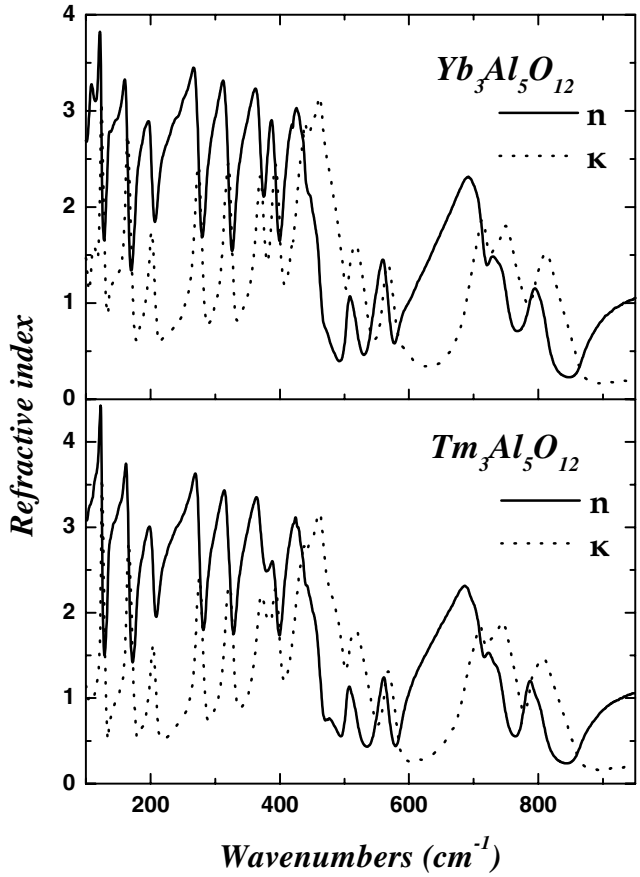

Figure 3. The real (n) and imaginary (κ) parts of the refractive index derived from Kramers–Kronig analysis for the $Tm_3Al_5O_{12}$ and $Yb_3Al_5O_{12}$ single crystals.

We would like to come back to the two T_{1u} missing modes. Our theoretical calculations, for both materials, predict that the set of T_{1u} modes must include vibrations at ∼375 and ∼96 cm^{-1} in accordance with the two additional weak IR peaks at ∼386 and 176 cm^{-1} reported for $Y_3Al_5O_{12}$ [4]. By taking into account the eigenvectors of the above two modes, obtained by our calculation and depicted in figure 5, we see that the participation of the RE ion in the displacements of the mode at 376 cm^{-1} is not significant, as it mainly exhibits a rotational character—e.g. the oxygen atoms are moving perpendicularly to their bonds with the cations. Therefore, it is anticipated that there will be only a small red-shift in going from the Y ion (atomic mass 88.9) to Tm (atomic mass 168.9) and Yb (atomic mass 173.0) ions. The situation is different for the IR modes at <200 cm^{-1}. Our theoretical calculations show that these modes involve a much higher degree of contribution from motions of the RE ions, which is in accordance with the experimental finding of McDevitt [2], who found a red-shift of these frequencies with increasing mass of the RE ion. Therefore the mode at ∼96 cm^{-1} observed for the Tm and Yb garnets may very well be one of the T_{1u} modes corresponding to the 176 cm^{-1} mode of the Y garnet. As regards the high-energy peaks, our calculations of the IR mode eigenvectors show that they are very complicated and correspond to mixtures of molecular modes, indicating a strong coupling of the polyhedra. This observation is in agreement with earlier results on the Raman mode eigenvectors [5].

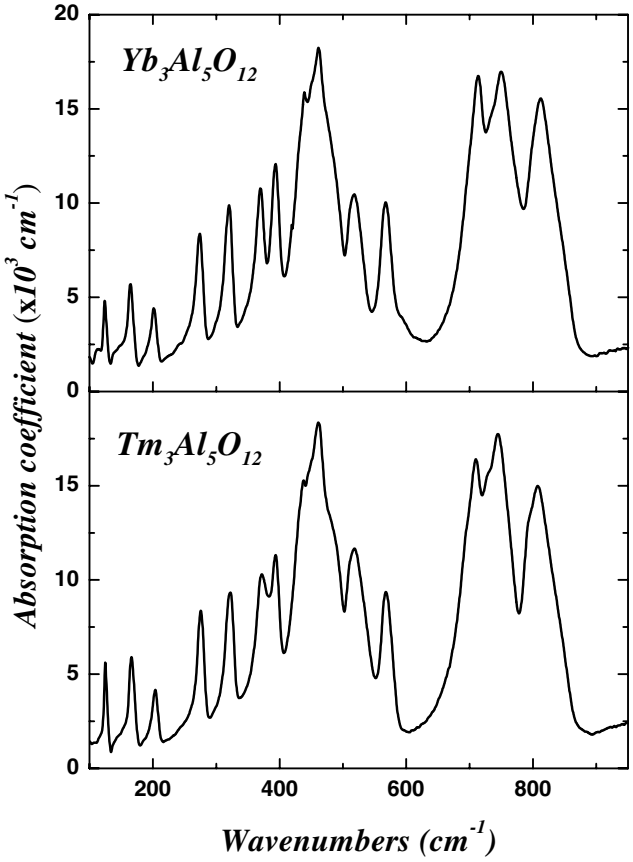

Figure 4. The absorption coefficient in the IR region for the $Tm_3Al_5O_{12}$ and $Yb_3Al_5O_{12}$ single crystals.

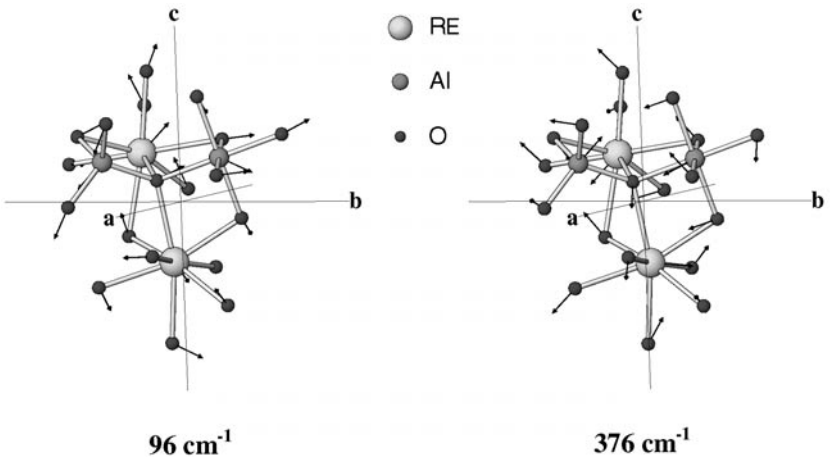

Figure 5. Eigenvectors for the T_{1u} modes at 96 and 376 cm^{-1}. In view of the complexity of the garnet structure, we present only the direction of the displacements of the basic polyhedra consisting of one tetrahedron, one octahedron, and two dodecahedra, which have a common oxygen. Note the higher contribution of the RE-atom displacement to the eigenvector of the mode at 96 cm^{-1}.

(This figure is in colour only in the electronic version)

Table 2. The effective charges, and the bond-stretching (L) and bond-bending (T) force constants calculated using the RIM for $Tm_3Al_5O_{12}$ and $Yb_3Al_5O_{12}$. The Z_i-parameters (i: Al(oct), Al(tetr), RE, OX) represent the effective charges of the tetrahedral and octahedral ions (Al(oct), Al(tetr)), the rare-earth ions (RE) and the oxygen ions (OX). The first-neighbour bond-stretching and bond-bending force constants are given for the Al–O bonds in the tetrahedra (L_{tetr}, T_{tetr}) and the octahedra (L_{oct}, T_{oct}) and for the RE–O bonds in the dodecahedra (L_{dod}, T_{dod}).

Parameters	$Tm_3Al_5O_{12}$	$Yb_3Al_5O_{12}$
e^- shells	[Xe] $4f^{13}6s^2$	[Xe] $4f^{14}6s^2$
m_{RE}	168.93	173.04
$Z_{Al(oct)}$ (e)	1.977	1.809
Z_{RE} (e)	1.997	2.160
$Z_{Al(tetr)}$ (e)	1.695	1.680
Z_{OX} (e)	−1.252	−1.262
L_{tetr} (N m^{-1})	413.51	416.81
L_{oct} (N m^{-1})	204.64	198.71
L_{dod} (N m^{-1})	178.85	189.82
T_{tetr} (N m^{-1})	40.48	40.18
T_{oct} (N m^{-1})	18.85	17.97
T_{dod} (N m^{-1})	16.87	17.74

The static (ε_o) and the high-frequency (ε_∞) dielectric constants are related to the IR frequencies through the Lyddane–Sachs–Teller (LST) relation [8, 9]

$$\prod_i \left(\frac{\omega_i(\mathrm{LO})}{\omega_i(\mathrm{TO})}\right)^2 = \frac{\varepsilon_o}{\varepsilon_\infty}. \tag{1}$$

The calculated values of the ratio $\varepsilon_o/\varepsilon_\infty$ are 3.17 for $Yb_3Al_5O_{12}$ and 3.20 for $Tm_3Al_5O_{12}$, in very good agreement with the experimental values of 3.9 and 4.0 for $Yb_3Al_5O_{12}$ and $Tm_3Al_5O_{12}$, respectively, deduced from our experimental ω_{TO}- and ω_{LO}-frequencies. ε_∞-values obtained independently, mainly from refractive index measurements in the visible region ($n^2 \sim \varepsilon_\infty$) [10], are 3.42 for $Yb_3Al_5O_{12}$ and 3.44 for $Tm_3Al_5O_{12}$. These values agree well with the corresponding values of 3.32 and 3.44 obtained from our reflectivity measurements at 4000 cm^{-1} for $Yb_3Al_5O_{12}$ and $Tm_3Al_5O_{12}$, respectively. The ε_o-values obtained through using the $\varepsilon_o/\varepsilon_\infty$ ratio are higher by a factor of 2 than those obtained through the Kramers–Kronig analysis of the dielectric function data (see figure 2), obviously because of low-limit restrictions in our measurements. A value around 10 for ε_o is found for other Y garnets [4], which seems to be correct also in our case if we consider our theoretical $\varepsilon_o/\varepsilon_\infty$ ratio values. The difference between the optic and static dielectric constants, $(\varepsilon_o - \varepsilon_\infty) \sim 6$, indicates a rather mixed character in the bond strengths of the whole crystal. This may be related to the presence of various types of bond and to the strongly coupled polyhedra in the garnet structure.

Finally, the absorption coefficient (figure 4) shows that the strongest IR lattice vibrations are lying in the high-frequency region (650–850 cm^{-1}) and in the frequency region 400–500 cm^{-1}. In contrast, the Raman spectra [5] have the strongest peaks between 350 and 450 cm^{-1}, while in the high-frequency region only the peak, which is assigned to the breathing mode of the tetrahedra and octahedra, exhibits significant intensity. By comparing the theoretically predicted IR and Raman eigenvectors (see figure 5 and [5]), we infer that the region 350–450 cm^{-1} is characterized by eigenmodes involving heavy mixing of rotational, translational, and the v_3 mode of the AlO_4 molecular unit.

References

[1] Powell R C 1998 *Physics of Solid State Laser Materials* (New York: AIP)
[2] McDevitt N T 1969 *J. Opt. Soc. Am.* **59** 1240
[3] Hurrell J P, Porto P S, Chang I F, Mitra S S and Bauman R P 1968 *Phys. Rev.* **173** 851
[4] Hofmeister A M and Campbell K R J 1992 *Appl. Phys.* **72** 638
[5] Papagelis K, Kanellis G, Kourouklis G A and Ves S 2002 *Phys. Status Solidi* b at press
[6] Menzer G 1928 *Z. Kristallogr.* **69** 300
[7] Bohr M and Huang K 1954 *Dynamical Theory of Crystal Lattices* (Oxford: Oxford University Press)
[8] Lyddane R H, Sachs R G and Teller E 1941 *Phys. Rev.* **59** 673
[9] Cochran W and Cowley R A 1962 *J. Phys. Chem. Solids* **23** 447
[10] Rubinstein C B and Barns R L 1965 *Am. Mineral.* **50** 782